In operando study of TiVCr additive in MgH2 composites

Laetitia Laversenne, Jérome Andrieux, Damien Planté, Laurence Lyard, Salvatore Miraglia

In operando study of TiVCr additive in MgH_2 composites

Laetitia Laversenne [a,b,], Jerome Andrieux [c,d], Damien Plante [a], Laurence Lyard [a], Salvatore Miraglia [a]*

[a] *Institut Ne´el, CNRS et Universite´ Joseph Fourier, BP 166, 38042 Grenoble, France*
[b] *Harvard University, School of Engineering and Applied Science, 02139 Cambridge, MA, USA*
[c] *ID15, ESRF, 6 rue Jules Horowitz, 38043 Grenoble, France*
[d] *Universite´ de Lyon, CNRS-UMR 5615 LMI, Lyon, France*

Keywords: Hydrogen storage, Magnesium hydride, TiVCr additive, Catalytic effect, In situ Synchrotron XRD.

ABSTRACT
We report an *in operando* study of the hydrogenation and dehydrogenation of MgH_2-TiVCr composites. The experiment was performed by means of *in situ* synchrotron XRD in order to get insights on the influence of the TiVCr additive on the sorption properties of the MgH_2 based composite. Sequential Rietveld refinement analysis was performed to investigate the structural changes of MgH_2 and of the additive during hydrogenation and dehydrogenation processes. Significant non-monotonic changes in the lattice volume of the $TiVCrH_x$ solid solution were observed concomitantly to the MgH_2 formation or decomposition. These volume changes are assigned to the variation of the hydrogen content in $TiVCrH_x$. These results provide evidence of cooperative effects between the H_2 storage material and the additive.

1. Introduction

Hydrogen is considered as one of the key components of sustainable development owing to high energy density (142 MJ kg^{-1}) and low environmental impact. Introducing this energy vector as a storage means for the leveling-out of power demand over time fulfills the necessity of saving energy, in particular in the case of renewable energy produced by intermittent sources. One of the major issues is to store H_2 safely and efficiently in a reversible hydride. Among the huge number of candidates for solid state storage, magnesium hydride has been studied for decades because of its high hydrogen capacity (7.6 wt.%), the abundance and relatively low cost of Mg, and the non-toxicity to humans and environment [1e4]. The weakness of MgH_2 is a relatively high thermodynamic stability (ΔH = -74.5 kJ/mol) [5] and a slow kinetics of hydrogen sorption. On-going researches directed at the destabilization of magnesium hydride are based on the formation of less thermodynamically stable hydrides of Mg rich intermetallic compounds [6-9] and on the nanoconfinement of MgH_2 in porous hosts [10,11]. Regarding the kinetics, significant enhancements have been observed on ball milled composites [12-14] with a large variety of additives, such as transition elements [15,16], intermetallic compounds [2,16-18], borides [19], oxides [20-22], and halides [23,24]. The key role of the microstructure of magnesium based composites was first reported by Gross et al., who demonstrated that both the reduction of the grain size resulting in an enlarged surface area, and the high degree of dispersion of the additives which act as a catalyst are responsible for enhanced hydrogenation and dehydrogenation kinetics [14,25]. In the case of the Mg/MgH_2 reaction, where the rate limiting step is the metal/hydride interface motion [26], the particles size reduction improves the sorption kinetics through an increased number of hydride nucleation sites located on the accessible surface. Moreover, the presence of the additives is responsible for a lowering of the dissociation energy of the hydrogen molecules and the enhancement of the diffusion rate of dissolved hydrogen atoms along the grain boundaries between Mg and the additives [18,25,27]. Reule et al. reported that optimized composites, in terms of high capacity and fast sorption kinetics, present a typical microstructure where the additive particles are covered by an MgH_2 thin film. In this case, the catalytic effect is mainly due to the MgH_2-additive interface [18]. Magnesium hydride composites with Ti-V based body centered cubic (bcc) alloys as an additive have been successfully implemented in large scale tanks [28,29]. In this type of composites, Yonkeu et al. showed that the hydrogenation kinetics is controlled by a three-dimensional growth of the hydride phase and the diffusion of hydrogen through the hydride phase. In contrast, the dehydrogenation kinetics is governed by the bulk/surface nucleation and two dimensional growth of the magnesium phase with a constant velocity of the Mg/MgH_2 interface [30]. Yu et al. suggested that the hydrogenated bcc alloy showed superior catalytic properties compared to the quenched bcc alloy in magnesium composites because the hydrogenation induces the formation of micro/nanosized additive particles [31] which greatly enhance the hydrogen atomic diffusivity. Thus, in order to provide insight into the catalytic role of the bcc additive in MgH_2 composites, previous studies have addressed microstructural [18], kinetical [30,32] and thermodynamical issues [16]. In this paper we investigate, *in operando*, the structural evolution of a TiVCr-MgH_2 composite upon hydrogenation and

dehydrogenation. The structural and chemical evolution of the composite was studied by using the time resolved and fast acquisition Synchrotron X-Ray Diffraction (Sync-XRD) on the ID15 beamline at ESRF in Grenoble. Structural refinement of the data was performed by means of sequential Rietveld analysis in order to determine the instantaneous behavior of both MgH_2 and the TiVCr additive.

2. Experimental details

The powders, MgH_2 (purity 98%) and 10 wt.% TiVCr ($Ti_{0.5}V_{1.9}Cr_{0.6}$ + 4 wt.% Zr_7Ni_{10} activating phase) were milled under Ar atmosphere in a Fritsch Pulverisette 5 planetary mill. WC balls and jars were used with a ball-to-powder ratio close to 1:20. A milling period of 60 min was applied with a rotational speed of 200 rpm. The handling of all powders was done in a glove box containing argon with O_2 and H_2O contents <1 ppm. *In situ* Sync-XRD measurements were performed at high energy (~90 keV) on the ID15 beamline at ESRF. The composite was introduced under the shape of compressed pellets in a 3 mm inner diameter sapphire capillary. The capillary was connected to a dedicated High-Pressure High-Temperature gas loading system fitted to an X-ray transparent furnace. The latter enables accurate sample temperature control during the diffraction experiment. The Pixium 4700 flat-panel detector was used with an exposure time of 1.6 s at a frequency of 5 s. A lead mask was specially designed and applied on the detector surface to shield the diffraction signal of the sapphire capillary. The beam size illuminating the sample was 0.3 x 0.3 mm^2. The exact wavelength, λ=0.1423(31) Å, was determined by using CeO_2 as a calibration reference. The diffraction pattern was obtained by radial integration of the raw image corrected from polarization and detector efficiency.

Fig. 1 describes the values of temperature and pressure during the *in operando* experiment. The experiment was composed of the following 4 sequences: (1) dehydrogenation of the fresh composite. The sample was heated up on a ramp of 20 °C/min up to 470 °C under a 2 bar argon flow (from pattern #1 to pattern #128). (2) Rehydrogenation at constant pressure and decreasing temperature. A pressure of 10 bar of hydrogen was applied in the fixed volume of the capillary and the tubing toward it and the sample was cooled down at a rate of 5 °C/min (from pattern #129 to #1240). (3) Dehydrogenation at constant pressure and increasing temperature. Once the temperature of 100 °C was reached, the atmosphere pressure was set to a continuous 2 bar Argon flow and the temperature was raised at a rate of 5 °C/min (from pattern #1241 to #2172) and, (4) cooling down of the dehydrogenated sample. Once the temperature of 470 °C was reached, a 15 min dwell time was applied (from pattern #2173 to #2231) and then the temperature was decreased at a set-up rate of 20 °C/min under 2 bar argon flow up to 117 °C (from pattern #2232 to #2730). During the experiment, a beam loss of 30 min occurred and consequently no patterns were recorded during the first dehydrogenation sequence. In other words, a period of time of 30 min separates pattern #128 and pattern #129. Similarly, the pure TiVCr additive was *in situ* characterized upon dehydrogenation performed under 2 bar argon flow up to 570 °C.

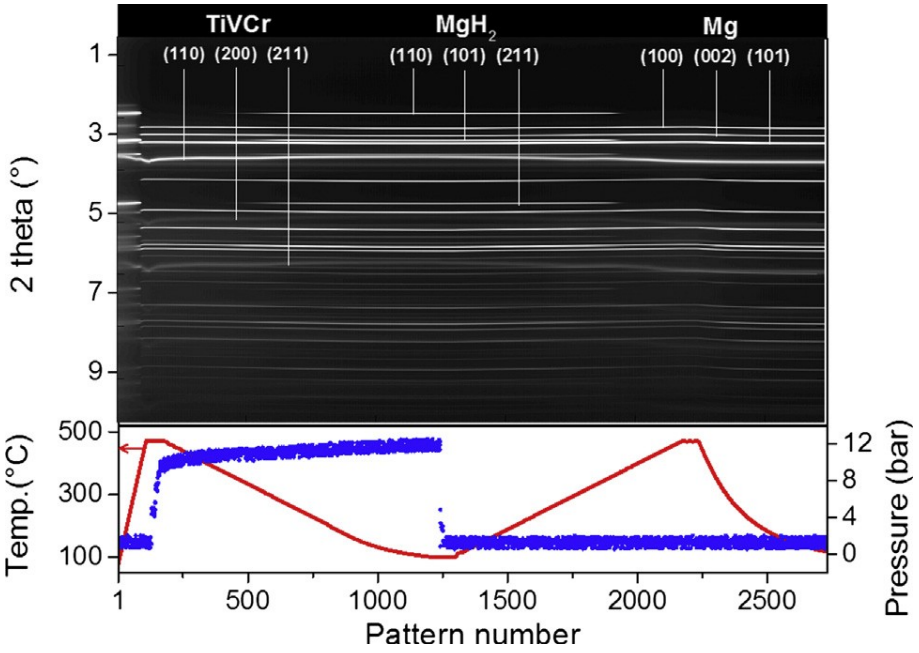

Fig. 1. *In situ* Sync-X-Ray diffraction performed on TiVCr-MgH_2 composite at the wavelength of λ = 0.1423 Å, the brighter the higher diffracted intensity (top) and experimental conditions (bottom). The sample temperature and pressure evolution are plotted as red line and blue dot respectively. Due to an inopportune synchrotron beam loss, the diffractograms collection was interrupted at pattern #128 during 30 min during the first high temperature dwell (meanwhile the temperature was maintained at 470 °C and the atmosphere was an Argon flow). It is the reason why the first dehydrogenation of the composite is only partially represented in the contour plot diagram.

The structural study was performed by Rietveld refinement using the FullProf Suite Software with the graphical interface WinPlotr [33,34]. Refined parameters for the sequential analysis included the lattice parameters, intensity scale factor, and background. The isotropic thermal factor and peak shape profile parameters were maintained constant. The background was refined using a 6th degree polynomial function. The profile function 7 in Full Prof, a Pseudo-Voigt function with axial divergence correction was employed. The instrument resolution file was defined with LaB_6. The precise temperature of the sample illuminated by the X-ray beam was calibrated by using the patterns of the last sequence of the *in operando* experiment (from pattern #2232 to #2730). For this purpose, the volume of the magnesium lattice was determined by Rietveld refinement as a function of the temperature measured by a thermocouple placed in the furnace. These values of temperature were then corrected regarding the tabulated value of magnesium thermal expansion [35]. Fig. 2 shows, as a function of the temperature, a comparison between the experimental results of the volume of the magnesium lattice and the data from the literature. A temperature shift of 50 °C was determined. Even if this temperature difference is large, we observed that the temperature ramp was well followed. The calibration was then systematically applied to the whole series of data given in this paper.

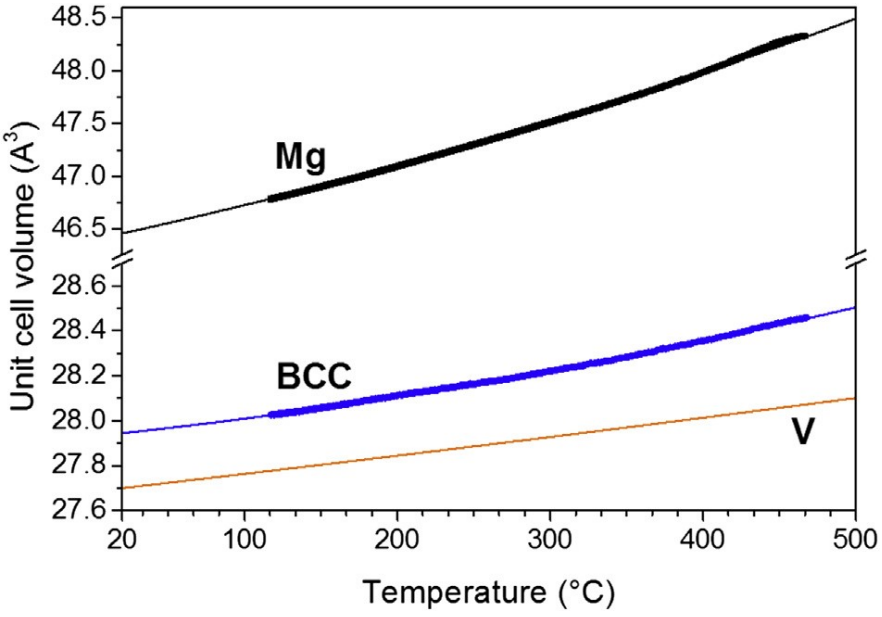

Fig. 2. Unit cell volume as function of temperature for Mg (black curves), bcc TiVCr (blue curves) and V (orange curve) phases. The thick curves correspond to experimental data refined on the fully dehydrogenated sample in the fourth sequence of the *in operando* experiment. The thin lines are the calculated values. In the case of Mg and V, the literature data given in Table 1 have been used to calculate the unit cell volume versus temperature. For the bcc phase, the thin line corresponds to the polynomial function fit of the experimental data, $V(T) = 27.93 \times (1 + 2.51\times10^{-5} \times T + 3.20\times10^{-8} \times T^2)$.

3. Results and discussion

3.1. *Dehydrogenation of the TiVCr additive*

Sync-XRD characterization has shown that the starting hydrogenated TiVCr additive is composed of two predominant phases which can be indexed in the face centered cubic (fcc) system, space group Fm-3m, and body centered cubic (bcc) system, space group Im-3m, respectively. Some authors have reported that the hydrogen poor solid solution formed in TiVCr alloys can be distorted in a body centered tetragonal phase (bct) as it has been observed in FeTiV alloys and in pure vanadium [36-40]. The angular resolution of the diffractograms and low diffraction intensity did not allow us to identify the bct structure. Fig. 3 shows the evolution of the fcc and bcc unit cell volumes versus temperature as determined by sequential Rietveld refinement during dehydrogenation of the pure TiVCr additive. The weight fraction of the bcc phase determined from the qualitative analysis is also plotted in Fig. 3. The observed dehydrogenation process of the additive is consistent with previous reports related to vanadium-based hydrides [39,41,42]. As shown in Fig. 3, in a first step (up to 260 °C), the two-phase domain (so called $\alpha + \beta$) is characterized by the thermal expansion of the two crystal lattices and a continuous decrease of the fcc weight fraction down to zero. Then (from ~280 °C to 570 °C in Fig. 3), the only phase in presence is the bcc solid solution $TiVCrH_x$ (so called α phase); its lattice volume monotonically decreases as the hydrogen content of the solid solution weakens.

3.2. In operando *experiment on the TiVCr-MgH_2 composite*

Fig. 1 combines the XRD patterns and the pressure and temperature in the course of the *in operando* experiment. For the sake of clarity, TiVCr (110), (200), (211), MgH_2 (110), (101), (211) and Mg (100), (002), (101) Bragg peaks positions are indicated in the contour plot diagram. Along the course of the four sequences of the *in operando* experiment (1: from pattern #1 to #128, dehydrogenation of the fresh composite, 2: from pattern #129 to #1240, rehydrogenation, 3: from pattern #1241 to #2231, dehydrogenation and 4: from pattern #2233 to #2730, cooling down), we observe large variations of the Bragg peaks positions, *i.e.* of the *d* spacings, of the TiVCr additive. The latter will be described in more detail in Section 3.4.

The profile of the Bragg peaks of the fresh composite is typical of ball milled samples where both reduction of the grain size and the presence of micro-strains lead to peak broadening and a decreased diffraction intensity. All the reflections of the Sync-XRD pattern recorded on the fresh composite at room temperature and ambient pressure (not shown here) have been indexed to the following phases: bcc and fcc $TiVCrH_x$ alloys, α- and γ-MgH_2 polymorphs and magnesium.

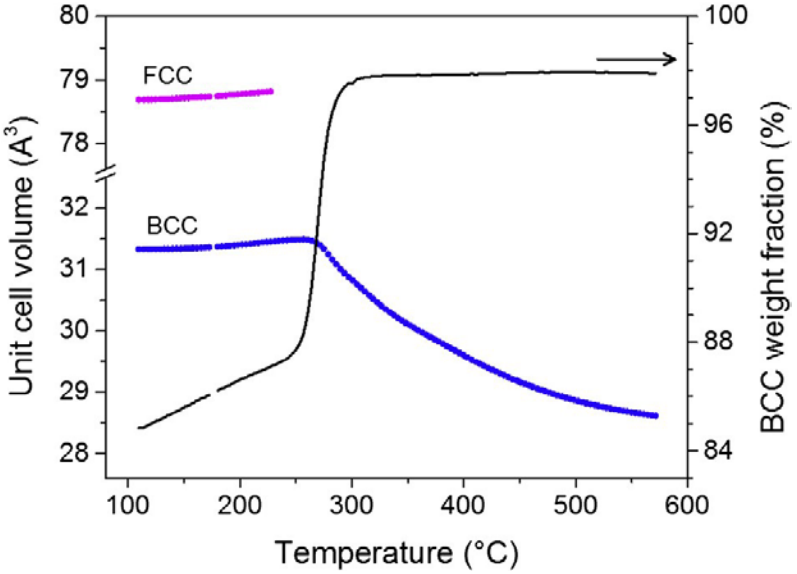

Fig. 3. Evolution of the fcc and bcc lattice parameters (magenta and blue curves respectively, left axis) and the bcc weight fraction (black curve, right axis) as a function of temperature during dehydrogenation of the pure TiVCr additive. Dehydrogenation was performed under 2 bar Ar flow from 100 °C to 570 °C at a heating rate of 5 °C/min.

The presence of residual magnesium is often observed in MgH_2 powders due to (1) the slow diffusion controlled hydride growth and (2) the probable presence of an oxide layer at the magnesium surface which is responsible for an even slower hydrogenation process [43-47]. Moreover, γ-MgH_2, the medium pressure polymorph of magnesium hydride is also observed in ball milled MgH_2 due to the relatively low activation energy of the α -> γ transformation [48]. The MgO phase cannot be identified in the XRD pattern for the fresh composite although its presence cannot be excluded. In fact, the appearance of MgO in course of the first heating ramp of the *in operando* experiment let us assume that MgO was already present in the fresh composite but not detectable because of the small quantity and well dispersion of this nearly amorphous phase. Fig. 1 shows that the broadening of the peaks observed in the fresh composite is reduced after the first heat treatment at 470 °C except for the TiVCr peaks which remain broad.

3.3. *Thermal behavior of the fully dehydrogenated composite*

As explained in the description of the experimental methods, the volume variation of the magnesium phase during the fourth sequence of the experiment was used to determine accurately the temperature at the position of the sample. This fourth sequence was also carried out to investigate the thermal expansion of the fully dehydrogenated TiVCr phase. The value of the solubility limit of hydrogen in hexagonal close packed (hcp) magnesium is discussed in several papers [49,50]. However, according to the majority of the works on the subject, within the temperature and pressure conditions of the *in operando* experiment, the hydrogen solubility in magnesium is expected to be lower than 1% [49,50]. Since the corresponding volume expansion is too small to be observed and quantified with the resolution of the diffraction patterns we have recorded, the magnesium phase has been considered with no solubilized hydrogen. Fig. 2 depicts the volume of Mg, MgO and TiVCr as a function of the temperature in the range 117 °C-470 °C. The dehydrogenated TiVCr lattice volume shown in Fig. 2 was fitted with the polynomial function: $V_0(T) =$

$27.93 + (7.01 \times 10^{-4})T + (8.95 \times 10^{-7})T^2$ for 100 °C < T < 470 °C where V is in Å^3 and T in °C. Extrapolation to the temperature of 20 °C gives a volume lattice of V_0 = 27.944 Å^3. The TiVCr lattice volume at room temperature corresponds to a lattice parameter of 3.031 Å, which is in very good agreement with the value reported by Miraglia et al. [51]. Pure vanadium lattice volume is also shown in Fig. 2 for comparison. The trend of increased thermal expansion upon Ti and Cr substitution in vanadium rich alloys compared to pure vanadium is on agreement with previous results [52].
An extrapolation of our results gives a mean expansion coefficient value of 13.6 x 10^{-6} per °C in the range 0-500 °C, which is slightly higher than the value of 10 x 10^{-6} per °C reported for macroscopic volumetric expansion of vanadium rich TiVCr alloys [52,53].

3.4. *Hydrogenation and dehydrogenation of TiVCr-MgH_2 composites*

Fig. 4 presents the Rietveld analysis of the Sync-XRD pattern #129 which was collected after a 35 min dwell time at 470 °C under a 2 bar argon flow.

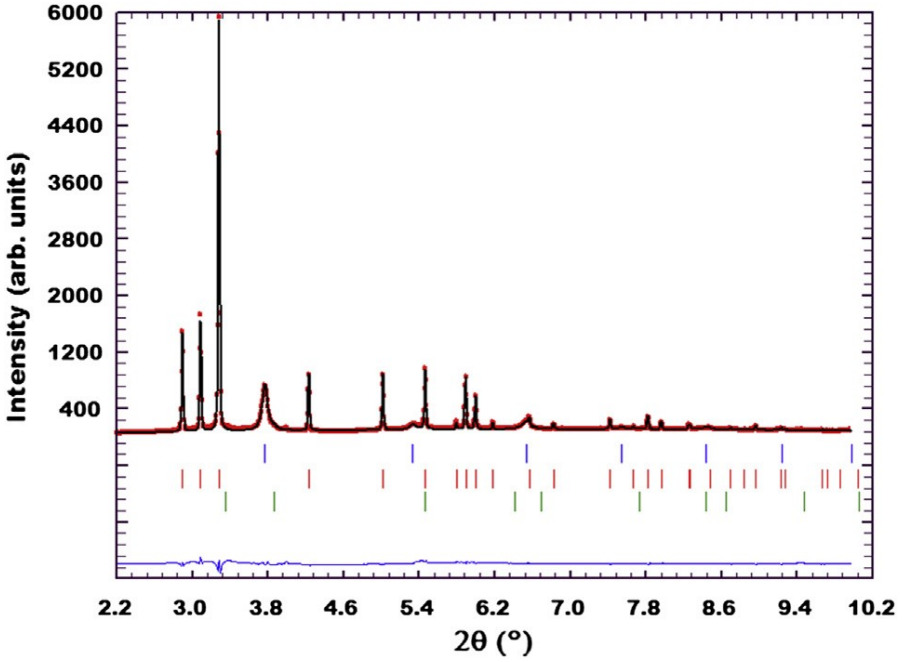

Fig. 4. Sync-XRD pattern of the dehydrogenated MgH_2-TiVCr composite at 470 °C, under Argon atmosphere (2 bar). The Rietveld analysis demonstrates the presence of body centered cubic hydrogenated $TiVCrH_x$ (s.g. Im-3m), hexagonal Mg (s.g. P63/mmc), and cubic MgO (s.g. Fm-3m). In the diagram, the red dot and the black continuous line show respectively the experimental and calculated diffraction profile whereas the blue line presents the difference between experimental and calculated profiles. The vertical lines indicate the Bragg peak positions of $TiVCrH_x$ (blue), MgH_2 (red) and MgO (green) respectively.

The structural refinement indicates that the composite is made up of 12.7 wt.% partially hydrogenated bcc $TiVCrH_x$ (s.g. Im-3m), 86.4 wt.% hexagonal Mg (s.g. P63/mmc) and 0.9 wt.% cubic MgO (s.g. Fm-3m). Hydrogenation of the composite was performed by applying a pressure of 10 bar of hydrogen while cooling down the sample at a set-up rate of 5 °C/min. Fig. 5 shows the Rietveld refinement of the pattern recorded at the end of this cooling ramp, when the temperature was 100 °C and the pressure was 10 bar of H_2. The quantitative phase analysis shows that the composite is partially hydrogenated and is composed of bcc $TiVCrH_x$ (9.15 wt.%), MgH_2 (21.65 wt.%), Mg (67.32 wt.%) and MgO (1.88 wt.%). The incomplete hydrogenation of the composite is due to the hydrogenation sequence which was too short given the slow sorption kinetics of magnesium. However, no evidence of the hydrogen rich face centered cubic (fcc) phase was observed in the experiment sequences which follow the dehydrogenation of the fresh composite. Thus the hydrogenated $TiVCrH_x$ phase was only described as a bcc lattice (s.g. Im-3m).
In order to investigate the role of the additive during the hydrogenation and dehydrogenation processes of Mg, sequential quantitative Rietveld analysis was performed. Figs. 6 and 7 present the unit cell volume of the phases in presence as a function of the temperature during hydrogenation and dehydrogenation. We observe that the lattice volume variations of MgO, MgH_2, and Mg are monotonic, continuous, and reversible during hydrogenation and dehydrogenation. The experimentally determined lattice volume variations can be directly related to the thermal expansion of the materials given in Table 1.

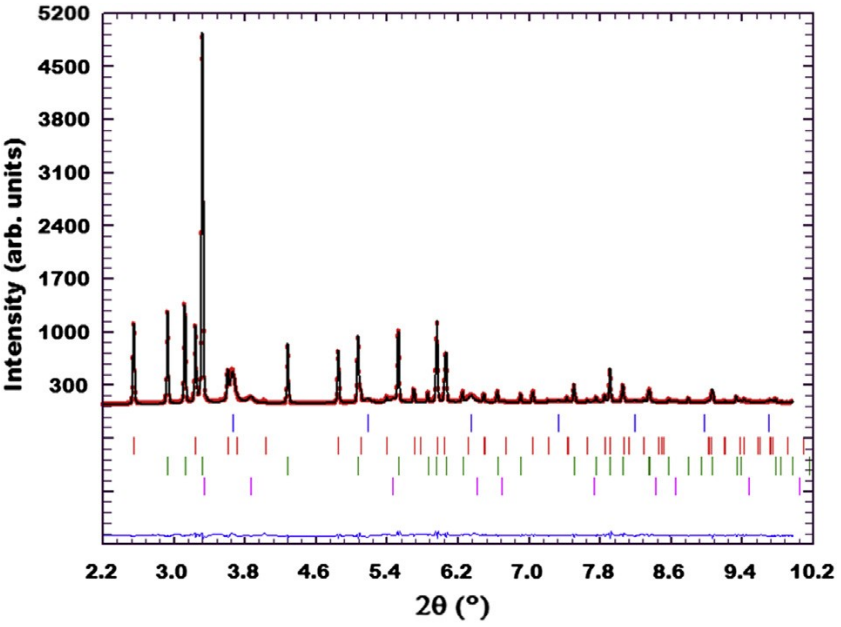

Fig. 5. Sync-XRD pattern of the MgH_2-TiVCr composite partially hydrogenated at 100 °C, under H_2 atmosphere (10 bar). The Rietveld analysis demonstrates the presence of body centered cubic hydrogenated $TiVCrH_x$ (s.g. Im-3m), orthorhombic MgH_2 (s.g. P42/mnm), hexagonal Mg (s.g. P63/mmc), and cubic MgO (s.g. Fm-3m). In the diagram, the red dot and the black continuous line show respectively the experimental and calculated diffraction profile whereas the blue line presents the difference between experimental and calculated profiles. The vertical lines indicate the Bragg peak positions of $TiVCrH_x$ (blue), MgH_2 (red), Mg (green) and MgO (pink) respectively.

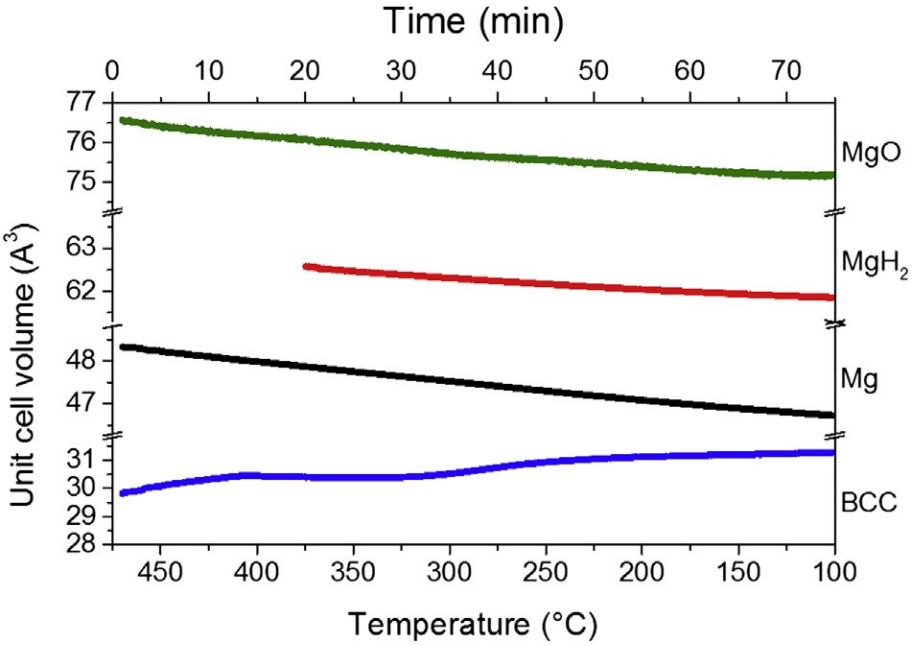

Fig. 6. Evolution of the unit cell volume of the components of the TiVCr-MgH_2 composite as a function of temperature during hydrogenation. Hydrogenation was performed under 10 bar H_2 by cooling down the temperature from 470 °C to 100 °C at rate of 5 °C/min.

Once again, the repeatability of the measurements testifies the good temperature control during the experiment. The behavior of the bcc phase volume differs from the others. The unit cell volume changes are in the opposite direction as what would be expected from thermal expansion. As described in Section 3.1 related to the pure additive, the decrease of the unit cell volume with increasing temperature is a result of the composition change of the bcc solid solution, *i.e.* the variation of the hydrogen content of the solid solution. The fast *in operando* diffractograms collection allows picturing the lattice volume changes of the $TiVCrH_x$ phase and reflects the instantaneous hydrogen content in the $TiVCrH_x$ solid solution. The hydrogen content of the $TiVCrH_x$ cannot be treated as an equilibrium value as the experiment is dynamical.

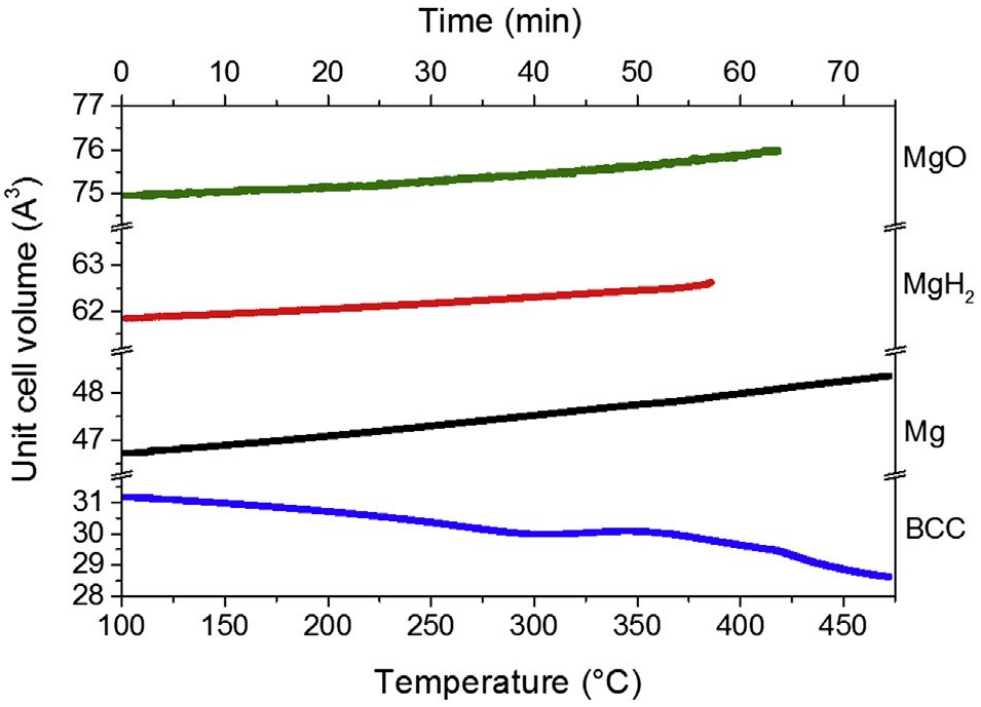

Fig. 7. Evolution of the unit cell volume of the components of the TiVCr-MgH_2 composite as a function of temperature during dehydrogenation. Dehydrogenation was performed under a 2 bar Ar flow by heating the sample from 100 °C to 470 °C at a rate of 5 °C/min.

Table 1. Volumetric thermal expansion of V, MgH_2 and Mg, according to literature data (at ambient pressure). The unit cell volume of MgH_2 versus temperature has been determined by first principle calculation; it explains why the given temperature range is larger than the existence domain range.

Material	Volumetric thermal expansion	References
V	$27.68456 \times (1 + 2.8221 \times 10^{-5} \times T + 2.9863 \times 10^{-9} \times T^2 + 1.5116 \times 10^{-12} \times T^3)$ for 25 °C < T < 2273 °C	[57]
MgH_2	$61.54567 \times (1 + 2.9897 \times 10^{-5} \times T + 4.7605 \times 10^{-8} \times T^2 - 4.9114 \times 10^{-13} \times T^3)$ for -273 °C < T < 727 °C	[58]
Mg	$46.39819 \times (1 + 6.6597 \times 10^{-5} \times T + 4.5818 \times 10^{-8} \times T^2 + 2.8325 \times 10^{-12} \times T^3)$ for 0 °C < T < 600 °C	[35]

Figs. 6 and 7 show the general trend of the $TiVCrH_x$ volume which reflects hydrogenation and dehydrogenation processes of the bcc solid solution. However, the bcc volume plotted as a function of the temperature shows a non-monotonic behavior which is not observed for Mg, MgH_2 and MgO. The $TiVCrH_x$ lattice expansion is also shown as a function of the temperature together with the MgH_2 weight fraction in Fig. 8 (hydrogenation) and Fig. 9 (dehydrogenation). We recall that the MgH_2 content was determined by Rietveld quantitative phase analysis. In Figs. 8 and 9, the $TiVCrH_x$ lattice expansion, for a given temperature, was defined as the ratio $(V - V_0)/V_0$ where V is the unit cell volume of the partially hydrogenated $TiVCrH_x$ phase and V_0 is the unit cell volume determined on the fully dehydrogenated composite (as described in Section 3.3). Our results show that the bcc lattice expansion varies in the range 4.8%-11.6% upon hydrogenation (Fig. 8) and 0.5%-11.2% upon dehydrogenation (Fig. 9). Although we cannot determine if the highest volume expansion reflects an equilibrium state of the hydrogenated $TiVCrH_x$ phase, the H/M (hydrogen/metal) ratio was calculated under the empirical observation that an interstitial hydrogen atom in transition metal alloys occupies an approximate volume of 2.2 $Å^3$ [54]. Considering the alloy unit cell volume equal to 28.01 $Å^3$ at 100 °C, a volume expansion of 11.6%, and taking into account that the TiVCr lattice contains 2 formula units, we obtained $x = 0.7$ as the H content of the solid solution. This estimated formula of $TiVCrH_{0.7}$ remains within the solubility limit of the alpha phase of vanadium hydride destabilized by Ti and Cr [55].

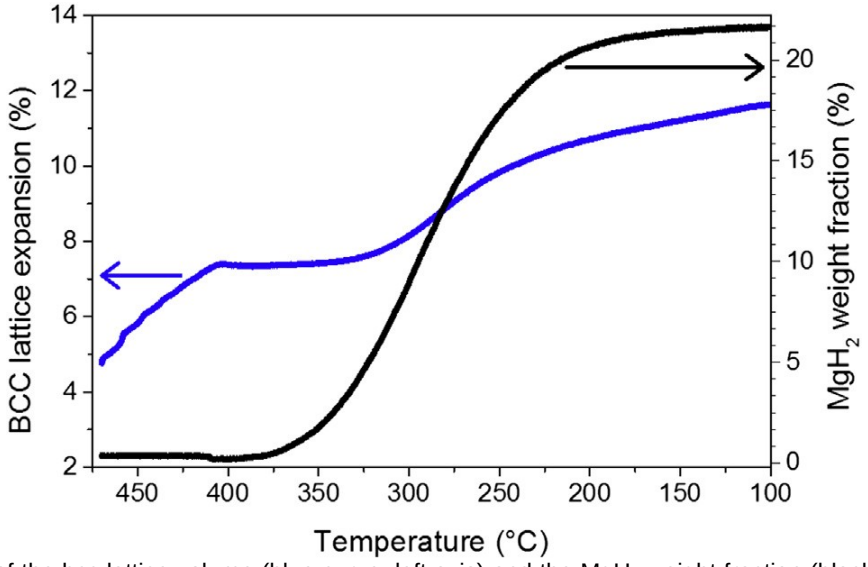

Fig. 8. Evolution of the bcc lattice volume (blue curve, left axis) and the MgH_2 weight fraction (black curve, right axis) as a function of temperature during hydrogenation. Hydrogenation was performed under 10 bar H_2 from 470 °C to 100 °C at a cooling rate of 5 °C/min.

Plotting the MgH_2 weight fraction together with the bcc lattice expansion allows us to show that the non-monotonic behavior of the $TiVCrH_x$ volume expansion occurs concomitantly with the startup change in MgH_2 content. In fact, Fig. 8 shows that the change in the slope of the $TiVCrH_x$ lattice expansion appears at 400 °C at the same time that MgH_2 starts to be formed upon cooling and, similarly, we observe that the MgH_2 decomposition at 300 °C is simultaneous with a change in the $TiVCrH_x$ lattice expansion upon dehydrogenation (Fig. 9). The previous experiment performed on the pure additive has shown that during the hydrogenation and dehydrogenation processes, the bcc $TiVCrH_x$ volume varies continuously and monotonically when similar experimental conditions are applied. Our results show that when the temperature and pressure reach the MgH_2 <-> Mg + H_2 equilibrium curve, it triggers a change in the hydrogen content of the $TiVCrH_x$ solid solution in the composite.

We assign the “breathing” of the $TiVCrH_x$ phase to be directly related to hydrogen exchange between the additive and Mg or MgH_2 at the scale of the grain in the composite rather than being due to a sudden change of the hydrogen partial pressure in the reactor vessel. Indeed, we have determined that upon dehydrogenation (Fig. 9), the highest rate of H_2 release occurs at the temperature of 368 °C as calculated by the first-degree derivative over the time of the MgH_2 weight fraction curve.

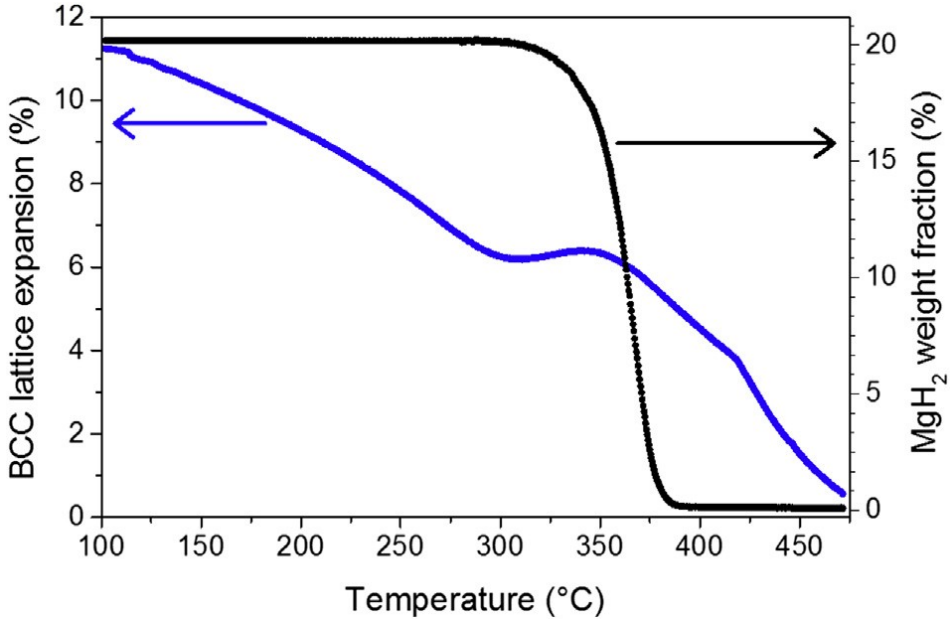

Fig. 9. Evolution of the bcc lattice parameter (blue curve, left axis) and the MgH_2 weight fraction (black curve, right axis) as a function of temperature during dehydrogenation. Dehydrogenation was performed under 2 bar Ar flow from 100 °C to 470 °C at a heating rate of 5 °C/min.

In the case that an overpressure of hydrogen occcurs in the reaction vessel, the $TiVCrH_x$ volume change should be the largest at that time of the experiment, but, our results show that the bcc volume change is monotonic within the temperature range 360 °C- 420 °C. Thus the present *in operando* study provides direct insight into the structural and chemical state of the additive during hydrogenation and dehydrogenation of magnesium hydride. The significant induced volume change of the additive is obviously playing a role in modifying the mechanical strains at the Mg-additive interface within the composite as shown previously [18,31]. It is useful to mention that the present experimental observations corroborate those of an earlier *in situ* EXAFS experiment [56] performed on bcc-doped MgH_2 where Nb was the activating phase. The formation of NbH_x clusters was revealed. The authors reached the conclusion that the H_2 desorption from MgH_2 is favored by local elastic stresses produced by β-$NbH_{0.89}$ clusters on the MgH_2 matrix that reduces the stability of the hydride phase. In order to establish whether $TiVCrH_x$ is a reaction intermediate acting as a gate for hydrogen sorption in Mg or whether it is just a spectator species, *in operando* isotherm experiments would be useful to complete the present dynamical study.

4. Conclusions

In this work, *in situ* Synchrotron XRD was used to determine the structural and chemical changes in a MgH_2 based composite activated with 10 wt.% TiVCr. The composite and the pure additive were studied *in operando* upon hydrogenation and dehydrogenation in order to investigate the catalytic effect of TiVCr. By determining the lattice thermal expansion of the additive, we were able to relate its unit cell volume to the hydrogen content of the $TiVCrH_x$ solid solution. While $TiVCrH_x$ shows a monotonic decrease in its volume upon dehydrogenation when studied as a pure material, it undergoes a sudden volume change concomitant with the MgH_2 decomposition in the composite. A similar behavior was observed upon hydrogenation of the composite where the change in the additive volume drops as the formation of MgH_2 occurs. These results provide evidence for a cooperative effect in the MgH_2 <-> $Mg + H_2$ reaction upon hydrogenation and dehydrogenation of the composite. The present study, which sheds light on the interaction between the additive and MgH_2, contributes to a better understanding of the catalytic mechanism occurring in this class of composites and could serve as a guide for designing efficient hydrogen storage systems.

5. Acknowledgments

The authors would like to acknowledge the ID15 staff at ESRF for the provision of beamtime and for the possibility to perform the *in operando* experiment. In particular, we thank V. Honkimaki and M. Di Michiel for their help with the macros for data analysis. We also thank A. Mauro, T. Buslaps and C. Chabert for their help in the implementation of the electronics and mechanics of the gas loading system.

6. References

[1] Vigeholm B, Kjøller J, Larsen B. Magnesium for hydrogen storage. Journal of the Less-Common Metals 1980;74:341e50.
[2] Tanguy B, Soubeyroux JL, Pezat M, Portier J, Hagenmuller P. Improvement of conditions for synthesizing magnesium hydride using adjuvants. Materials Research Bulletin 1976;11:1441e7.
[3] Jain IP, Lal C, Jain A. Hydrogen storage in Mg: a most promising material. International Journal of Hydrogen Energy 2010;35:5133e44.
[4] Bogdanovic B. Magnesium hydride e a homogeneous- catalyzed synthesis and its use in hydrogen storage. International Journal of Hydrogen Energy 1984;9:937e41.
[5] Stampfer JF, Holley CE, Suttle JF. The magnesium hydrogen system. Journal of the American Chemical Society 1960;82:3504e8.
[6] Ponthieu M, Fernandez JF, Cuevas F, Ares JR, Leardini F, Bodega J, et al. Reversible hydrogen storage in the Ni-rich pseudo-binary $Mg_6Pd_{0.25}Ni_{0.75}$ intermetallic compound: reaction pathway, thermodynamic and kinetic properties. Journal of Alloys and Compounds 2013;548:96e104.
[7] Sato T, Kyoi D, Ronnebro E, Kitamura N, Sakai T, Noreus D. Structural investigations of two new ternary magnesiumeniobium hydrides, $Mg_{6.5}NbH$ similar to 14 and $MgNb_2H$ similar to 4. Journal of Alloys and Compounds 2006;417:230e4.
[8] Kyoi D, Sato T, Ronnebro E, Tsuji Y, Kitamura N, Ueda A, et al.
A novel magnesium-vanadium hydride synthesized by a gigapascal-high-pressure technique. Journal of Alloys and Compounds 2004;375:253e8.
[9] Couillaud S, Gaudin E, Weill F, Gomez S, Stan C, Plante D, et al. Structure of a new ternary compound with high magnesium content, so-called $Gd_{13}Ni_9Mg_{78}$. Acta Materialia 2012;60:4144e51.
[10] de Jongh PE, Wagemans RWP, Eggenhuisen TM,
Dauvillier BS, Radstake PB, Meeldijk JD, et al. The preparation of carbon-supported magnesium nanoparticles using melt infiltration. Chemistry of Materials 2007;19:6052e7.
[11] Lim DW, Yoon JW, Ryu KY, Suh MP. Magnesium nanocrystals embedded in a metal-organic framework: hybrid hydrogen storage with synergistic effect on physiand chemisorption. Angewandte Chemie International Edition 2012;51:9814e7.
[12] Lu J, Choi YJ, Fang ZZ, Sohn HY, Ronnebro E. Hydrogen storage properties of nanosized MgH_2e0.1TiH(2) prepared by ultrahigh-energy-high-pressure milling. Journal of the American Chemical Society 2009;131:15843e52.
[13] Jeon K-J, Moon HR, Ruminski AM, Jiang B, Kisielowski C, Bardhan R, et al. Air-stable magnesium nanocomposites provide rapid and

high-capacity hydrogen storage without using heavy-metal catalysts. Nature Materials 2011;10:286e90.
[14] Gross KJ, Spatz P, Zuttel A, Schlapbach L. Mg composites for hydrogen storage e the dependence of hydriding properties on composition. Journal of Alloys and Compounds 1997;261:276e80.
[15] Liang G, Huot J, Boily S, Schulz R. Hydrogen desorption kinetics of a mechanically milled MgH(2)5at.%V nanocomposite. Journal of Alloys and Compounds 2000;305:239e45.
[16] Liang G, Huot J, Boily S, Van Neste A, Schulz R. Catalytic effect of transition metals on hydrogen sorption in nanocrystalline ball milled MgH_2eTm (Tm = Ti, V, Mn, Fe and Ni) systems. Journal of Alloys and Compounds 1999;292:247e52.
[17] Liang G, Huot J, Boily S, Van Neste A, Schulz R. Hydrogen storage in mechanically milled MgeLaNi5 and MgH_2eLaNi5 composites. Journal of Alloys and Compounds 2000;297:261e5.
[18] Reule H, Hirscher M, Weisshardt A, Kronmuller H. Hydrogen desorption properties of mechanically alloyed MgH_2 composite materials. Journal of Alloys and Compounds 2000;305:246e52.
[19] Dobrovolsky VD, Ershova OG, Solonin YM, Khyzhun OY, Paul-Boncour V. Influence of TiB_2 addition upon thermal stability and decomposition temperature of the MgH_2 hydride of a Mg-based mechanical alloy. Journal of Alloys and Compounds 2008;465:177e82.
[20] Hanada N, Ichikawa T, Isobe S, Nakagawa T, Tokoyoda K, Honma T, et al. X-ray absorption spectroscopic study on valence state and local atomic structure of transition metal oxides doped in MgH_2. Journal of Physical Chemistry C 2009;113:13450e5.
[21] Dolci F, Di Chio M, Baricco M, Giamello E. Niobium pentoxide as promoter in the mixed MgH_2/Nb_2O_5 system for hydrogen storage: a multitechnique investigation of the H-2 uptake. Journal of Materials Science 2007;42:7180e5.
[22] Wang P, Wang AM, Zhang HF, Ding BZ, Hu ZQ. Hydrogenation characteristics of MgeTiO2 (rutile) composite. Journal of Alloys and Compounds 2000;313:218e23.
[23] Grzech A, Lafont U, Magusin P, Mulder FM. Microscopic study of TiF_3 as hydrogen storage catalyst for MgH_2. Journal of Physical Chemistry C 2012;116:26027e35.
[24] Al-Kukhun A, Hwang HT, Varma A. NbF_5 additive improves hydrogen release from magnesium borohydride. International Journal of Hydrogen Energy 2012;37:17671e7. [25] Gross KJ, Chartouni D, Leroy E, Zuttel A, Schlapbach L. Mechanically milled Mg composites for hydrogen storage: the relationship between morphology and kinetics. Journal of Alloys and Compounds 1998;269:259e70.
[26] Huot J, Liang G, Boily S, Van Neste A, Schulz R. Structural study and hydrogen sorption kinetics of ball-milled magnesium hydride. Journal of Alloys and Compounds 1999;293:495e500.
[27] von Zeppelin F, Reule H, Hirscher M. Hydrogen desorption kinetics of nanostructured MgH_2 composite materials. Journal of Alloys and Compounds 2002;330:723e6.
[28] Delhomme B, de Rango P, Marty P, Bacia M, Zawilski B, Raufast C, et al. Large scale magnesium hydride tank coupled with an external heat source. International Journal of Hydrogen Energy 2012;37:9103e11.
[29] Garrier S, Chaise A, de Rango P, Marty P, Delhomme B, Fruchart D, et al. MgH_2 intermediate scale tank tests under various experimental conditions. International Journal of Hydrogen Energy 2011;36:9719e26.
[30] Yonkeu AL, Swainson IP, Dufour J, Huot J. Kinetic investigation of the catalytic effect of a body centered cubic- alloy $TiV_{1.1}Mn_{0.9}$ (BCC) on hydriding/dehydriding properties of magnesium. Journal of Alloys and Compounds 2008;460:559e64.
[31] Yu XB, Yang ZX, Liu HK, Grant DM, Walker GS. The effect of a TieV-based BCC alloy as a catalyst on the hydrogen storage properties of MgH_2. International Journal of Hydrogen Energy 2010;35:6338e44.
[32] Hu YQ, Yan C, Zhang HF, Ye L, Hu ZQ. Preparation and hydrogenation characteristics of Mg-30 wt.% $Ti_{37.5}V_{25}Cr_{37.5}$ composite. Journal of Alloys and Compounds 2004;375:265e9.
[33] Rodrı´guez-Carvajal J. Recent advances in magnetic structure determination by neutron powder diffraction. Physica B: Condensed Matter 1993;192:55e69.
[34] Roisnel T, Rodriguez-Carvajal J. WinPLOTR: a Windows tool for powder diffraction pattern analysis. In: Delhez R, Mittemeijer EJ, editors. Epdic 7: European powder diffraction, Pts 1 and 22001. p. 118e123.
[35] Avedesian MM, Baker Hugh. Magnesium and magnesium alloys. ASM International; 1999.
[36] Kawasuso A, Arashima H, Maekawa M, Itoh H, Kabutomori T. TiCrV hydrogen storage alloy studied by positron annihilation spectroscopy. Journal of Alloys and Compounds 2009;486:278e83.
[37] Cho SW, Enoki H, Kabutomori T, Park CN, Akiba E. Isotope effect on structural transitions of $Ti_{1.0}Mn_{0.9}V_{1.1}H_x$(D-*X*) and $Ti_{1.0}Cr_{1.5}V_{1.7}H_x$(D-*X*) with hydrogenation. Journal of Alloys and Compounds 2001;319:196e203.
[38] Massicot B, Latroche M, Joubert JM. Hydrogenation properties of FeeTieV bcc alloys. Journal of Alloys and Compounds 2011;509:372e9.
[39] Tamura T, Kazumi T, Kamegawa A, Takamura H, Okada M. Effects of protide structures on hysteresis in TieCreV protium absorption alloys. Materials Transactions 2002;43:2753e6.
[40] Tsukahara M. Hydrogenation properties of vanadium-based alloys with large hydrogen storage capacity. Materials Transactions 2011;52:68e72.
[41] Tamura T, Kazumi T, Kamegawa A, Takamura H, Okada M. Protium absorption properties and protide formations of TieCreV alloys. Journal of Alloys and Compounds 2003;356:505e9.
[42] Akiba E, Iba H. Hydrogen absorption by Laves phase related BCC solid solution. Intermetallics 1998;6:461e70.
[43] Gerasimov KB, Konstanchuck IG, Chizhik SA, Bobet JL. "Hysteresis" in interaction of nanocrystalline magnesium with hydrogen. International Journal of Hydrogen Energy 2009;34:1916e21.
[44] Zaluska A, Zaluski L, Strom-Olsen JO. Nanocrystalline magnesium for hydrogen storage. Journal of Alloys and Compounds 1999;288:217e25.
[45] Krozer A, Kasemo B. Equilibrium hydrogen uptake and associated kinetics for the $MgeH_2$ system at low-pressures. Journal of Physics-Condensed Matter 1989;1:1533e8.
[46] Vigeholm B, Jensen K, Larsen B, Pedersen AS. Elements of hydride formation mechanisms in nearly spherical magnesium powder particles. Journal of the Less-Common Metals 1987;131:133e41.
[47] Vigeholm B, Kjoller J, Larsen B, Pedersen AS. Formation and decomposition of magnesium hydride. Journal of the Less- Common Metals 1983;89:135e44.
[48] Vajeeston P, Ravindran P, Hauback BC, Fjellvag H, Kjekshus A, Furuseth S, et al. Structural stability and pressure-induced phase transitions in MgH_2. Physical Review B 2006;73.
[49] Bohmhammel K, Wolf U, Wolf G, Konigsberger E. Thermodynamic optimization of the system magnesiumehydrogen. Thermochimica Acta 1999;337:195e9.
[50] Zeng K, Klassen T, Oelerich W, Bormann R. Critical assessment and thermodynamic modeling of the MgeH system. International Journal of Hydrogen Energy 1999;24:989e1004. [51] Miraglia S, de Rango P, Rivoirard S, Fruchart D, Charbonnier J, Skryabina N. Hydrogen sorption properties of compounds based on BCC Ti(1-*x*)V(1-*y*)Cr(1 þ *x*þ *y*) alloys. Journal of Alloys and Compounds 2012;536:1e6.

[52] Yaggee FL, Gilbert ER, Styles JW. Thermal expansivities, thermal conductivities, and densities of vanadium, titanium, chromium and some vanadium-base alloys e (a comparison with austenitic stainless STEEL). Journal of the Less- Common Metals 1969;19:39e51.
[53] Smith DL, Loomis BA, Diercks DR. Vanadium-base alloys for fusion-reactor applications e a review. Journal of Nuclear Materials 1985;135:125e39.
[54] Fukai Y. From metal hydrides to the metal-hydrogen system.
Journal of the Less-Common Metals 1991;172e174:8e19. [55] Yukawa H, Yamashita D, Ito S, Morinaga M, Yamaguchi S.
Compositional dependence of hydriding properties of vanadium alloys at low hydrogen pressures. Journal of Alloys and Compounds 2003;356:45e9.
[56] Checchetto R, Bazzanella N, Miotello A, Maurizio C, D'Acapito F, Mengucci P, et al. Nb clusters formation in Nb-doped magnesium hydride. Applied Physics Letters 2005;87.
[57] Cindas LLC database. https://cindasdatacom.
[58] Kelkar T, Kanhere DG, Pal S. First principles calculations of thermal, equations of state and thermodynamical properties of MgH(2) at finite temperatures. Computational Materials Science 2008;42:510e6.